Research Article
doi.org/10.1002/cbic.202200795
Chemistry Europe
European Chemical Societies Publishing

www.chembiochem.org

FerryCalin: an Engineered Lipocalin Protein Directed against the Transferrin Receptor with Potential for Brain Drug Delivery

Lea Nästle[+],[a] Friedrich-Christian Deuschle[+],[a] Volker Morath,[a] and Arne Skerra*[a]

The transferrin receptor (TfR) mediates transcytosis across the blood-brain barrier (BBB), which offers a promising approach for the non-invasive delivery of therapeutics into the brain parenchyma. Employing the recombinant homodimeric murine TfR ectodomain, prepared in a biochemically functional state, we have selected a cognate Anticalin via phage display and bacterial cell surface display from a random library based on the human lipocalin 2 (Lcn2). After affinity maturation, several engineered lipocalin variants were identified that bind murine TfR in a non-competitive manner with the natural ligand (transferrin·Fe^{3+}), among those an Anticalin – dubbed FerryCalin – exhibiting a dissociation constant (K_D) of 3.8 nM. Epitope analysis using the SPOT technique revealed a sequential epitope in a surface region of TfR remote from the transferrin-binding site. Due to the fast k_{on} rate and short complex half-life, as evidenced by real-time surface plasmon resonance (SPR) measurements, FerryCalin, or one of its related mutants, shows characteristics as a potential vehicle for the brain delivery of biopharmaceuticals.

Introduction

The blood-brain barrier (BBB) represents a cellular interface between the vasculature and the central nervous system (CNS) which prevents the entry of circulating substances into the CNS, including many pharmacologically active compounds, or tightly regulates their exchange between the blood and the brain parenchyma.[1] Apart from small molecule drugs, the BBB also restricts the delivery of biopharmaceuticals. For instance, less than 0.1% of full-length IgG antibodies get distributed into the brain after peripheral administration.[2] Thus, effective passage of the BBB constitutes one of the major obstacles for the development of potent neuropharmaceuticals to treat both original diseases of the CNS, such as Parkinson's and Alzheimer's disease, or diseases with a pathologically relevant manifestation within the brain, like Hunter's syndrome.

A promising approach to non-invasively traverse the intact BBB exploits endogenous receptor-mediated transcytosis (RMT) at the brain capillary endothelium.[3] In this approach, a ligand (e.g., a binding protein or peptide) specific for a suitable transcytosis receptor whose extramembrane domain is accessible at the luminal side of the endothelial cells is conjugated – as a kind of shuttle compound – with a pharmacologically active cargo molecule (e.g., a monoclonal antibody, enzyme, peptide or small molecule) to mediate transport into the brain. So far, the most promising RMT targets for this endeavour comprise the transferrin receptor 1 (TfR),[4] the insulin receptor (IR)[5] and the CD98 heavy chain (CD98hc),[6] which all have been addressed successfully to enable a more efficient brain delivery of drug candidates.

Among these, the most extensively studied target is the TfR (CD71). TfR plays a central physiological role in the maintenance of cellular iron homeostasis, including iron delivery to the CNS, and is exposed in high abundance on brain endothelial cells.[7] Several TfR-specific antibodies or modified Ig proteins[8] as well as peptides[9] have been developed for brain drug delivery of therapeutic or diagnostic agents, however with varying success. For example, the murine antibody OX-26 specific for the rat TfR[7b,10] and the rat monoclonal antibody 8D3 specific for the murine ortholog[11] were both shown to target this receptor in vivo without interfering with binding of the natural ligand transferrin (Tf), followed by internalization into the brain endothelial cells and transport into the brain parenchyma. Of note, despite a partially overlapping binding site with heavy-chain ferritin – which provides an alternative or additional physiological source of bioavailable iron compared to Tf – as deduced from a single-particle cryo-electron microscopy structure of the human protein complex,[12] the 8D3 antibody conferred high BBB permeability in mice when applied in various fusion protein formats.[11b–d] This is consistent with the fact that the same binding region on human TfR is also targeted by arenaviruses and *Plasmodium vivax* for cellular entry.[12]

On the other hand, recent studies performed with derivatives of these two mAbs indicated that both a moderate (nanomolar) affinity towards TfR and a monovalent binding mechanism are critical factors for the successful transcellular

[a] *L. Nästle,[+] Dr. F.-C. Deuschle,[+] V. Morath, Prof. Dr. A. Skerra*
Lehrstuhl für Biologische Chemie
Technische Universität München
85354 Freising (Germany)
E-mail: skerra@tum.de

[+] *These authors contributed equally to this work.*

Supporting information for this article is available on the WWW under https://doi.org/10.1002/cbic.202200795

trafficking across the endothelial cell layer.[4,13] Apparently, slow dissociation kinetics and an avidity effect (arising from the bivalent nature of conventional antibodies) both hamper efficient release on the brain parenchymal side. Furthermore, the absence of Fc-mediated effector functions – thus preventing unwanted immunological side effects[14] – as well as the specific formatting of the shuttle and cargo moieties are relevant factors for the viable design of fusion proteins to develop BBB-penetrating neurobiologics.

Anticalins constitute a class of clinical-stage engineered binding proteins based on a human lipocalin scaffold which appear promising to meet these requirements.[15] Here, we present the selection and characterization of a novel Anticalin directed towards the extracellular domain of murine TfR (muTfR-ED). The demonstrated favorable biochemical and binding characteristics make it a good candidate for brain drug delivery when combined with a suitable biopharmaceutical as conjugate or in a fusion protein, optionally via a flexible linker.

Results and Discussion

Development of an expression system for the muTfR ectodomain

Transient heterologous production of the homodimeric muTfR-ED (UniProt ID Q62351, residues Cys^{89}-Phe^{763}) was accomplished in MEXi-293E HEK cells using the plasmid pDSG-BM40-His$_6$-BAP-muTfR-ED-Igk-BirA-*Strep*DEL (Figure 1). This plasmid encodes the sequence for the ectodomain of the murine TfR with an N-terminal signal peptide (BM40) N-terminally fused with a His$_6$-tag and a biotin acceptor peptide (BAP; amino acid sequence: GLNDIFEAQKIEWHE).[16] To prevent potential formation of non-physiological interchain disulfide bridges within the stalk region of the type 2 transmembrane receptor upon dimerization, the Cys residue at position 89 was mutated to Ser such that only Cys^{98} was retained, thus resulting in a single disulfide crosslink between the paired ectodomains (Figure 1F).

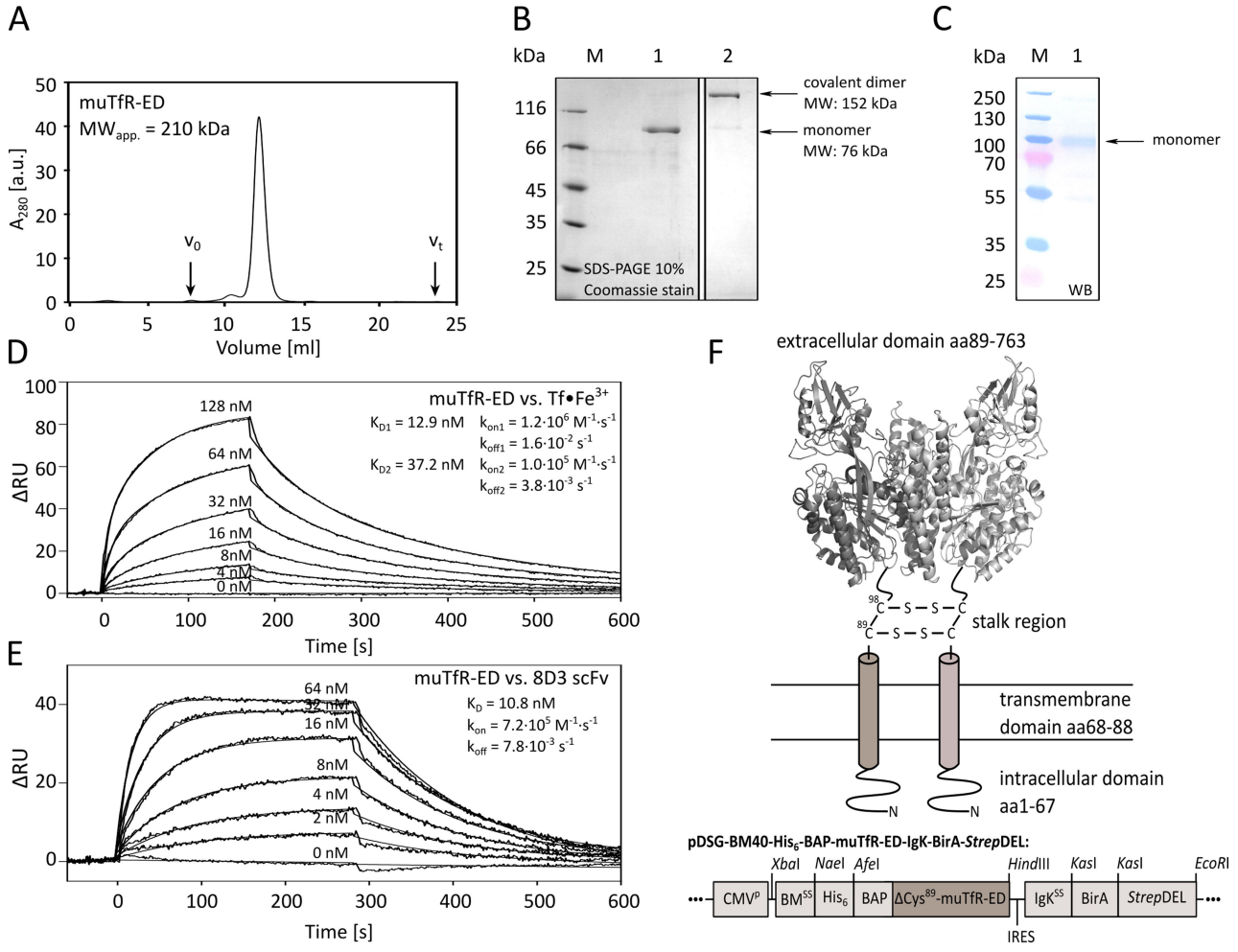

Figure 1. Preparation and characterization of the recombinant muTfR-ED. (A) Analytical SEC of the glycosylated muTfR-ED purified from HEK cells. (B) SDS-PAGE and (C) western blot analysis of muTfR-ED, confirming disulfide-mediated homodimer formation as well as covalent biotin attachment (M: Marker; 1: reducing condition; 2: not reduced; WB: western blot using ExtrAvidin-AP under reducing condition). SPR interaction analysis of immobilized muTfR-ED (ΔRU ~800) with muTf·Fe^{3+} (D) or with the 8D3 scFv fragment (E). (F) Schematic illustration of the disulfide-crosslinked TfR1 homodimer and of the plasmid construct used for the soluble expression of its glycosylated ectodomain. The plasmid pDSG-BM40-His$_6$-BAP-muTfR-ED-Igk-BirA-*Strep*DEL carries the following functional elements: CMV^p, cytomegalovirus promoter; BM^{ss} and Igk^{ss}, signal sequences for protein secretion; His$_6$, affinity tag; BAP, biotin acceptor peptide; IRES, internal ribosome entry site; *Strep*DEL, a combined *Strep*-tag II and KDEL ER retention sequence (WSHPQFE**KDEL**).

The bicistronic construct, separated by an internal ribosome entry site,[17] also enabled co-expression of the biotin protein ligase BirA (EC: 6.3.4.15) to catalyze biotin attachment to the ε-amino group of the single Lys residue within the BAP at the N-terminus of muTfR-ED.[16a] BirA was expressed with a so-called *Strep*DEL-tag at its C-terminus, a chimera between the *Strep*-tag II (amino acid sequence: WSHPQFEK)[18] and the endoplasmic reticulum (ER) retention sequence (KDEL).[19] This bifunctional peptide tag allowed both detection of the expressed enzyme via the *Strep*-tag II (e.g., on a western blot of a cell lysate) and its intracellular localisation within the ER, that is on the secretory pathway of muTfR-ED. By exploiting the strong molecular interaction with (strept)avidin, it was subsequently possible to immobilize the purified biotinylated muTfR-ED on appropriately functionalized surfaces (e.g. magnetic beads, plastic surfaces or sensor chips) with its membrane-distal extracellular part exposed.

The biotinylated muTfR-ED was isolated from the cell culture supernatant and purified to homogeneity by IMAC and SEC. Analytical SEC revealed an apparent molecular size of the homodimer of 210 kDa, which is by ~40% larger than the calculated mass of 152 kDa. This effect can be attributed to the multiple glycosylation at positions Asn^{253}, Asn^{319} and Asn^{725} in each subunit[20] (Figure 1A). SDS-PAGE under non-reducing conditions and western blot analysis, respectively, confirmed covalent dimer formation as well as attachment of the biotin group (Figure 1B and C). SPR analysis of the muTfR-ED bound to a sensorchip by applying its natural ligand muTf·Fe^{3+} in the mobile phase, as well as a single chain variable fragment (scFv) derived from the cognate antibody 8D3[11a,21] (cf. Figure S1), confirmed high binding activity in each case, with K_D values similar to those published (Figure 1D and E).[11c,22] Of note, the correct assembly of the homodimeric muTfR-ED is a known prerequisite for the tight interaction with muTf·Fe^{3+}.[23]

Selection of TfR-specific Anticalins from a combinatorial lipocalin library

Selection of Anticalins directed against muTfR was accomplished employing the human Lcn2 scaffold with 20 amino acid positions randomized in a targeted manner.[24] This genetic random library, having a combinatorial complexity of approximately $1x10^{10}$, was previously applied to select Anticalins against several targets with biomedical relevance.[25] For the selection of TfR-specific lipocalin variants, six cycles of filamentous phage display were performed.

During this selection process the Tf-binding site on the purified muTfR-ED target was shielded by forming a complex with muTf·Fe^{3+} in order to specifically enrich lipocalin variants that bind in a non-competitive manner with the natural receptor ligand. This strategy was chosen under three aspects: i) the Tf concentration in blood is ~25 μM[26] and, thus, TfR is fully saturated under physiological conditions; ii) TfR undergoes a conformational change upon complex formation with Tf,[23] which may obscure conformational epitopes; iii) the Anticalin should not compete with normal cellular iron transport under conditions of high dosing, for example during chronic therapy. On the other hand, the muTfR-ED was applied in the absence of muTf·Fe^{3+} for the subsequent ELISA screening in order to potentially identify also those Anticalins that may recognize the TfR independently of conformational changes triggered by muTf binding.

After six cycles of Anticalin phage display selection, the enrichment of a phagemid subpopulation with pronounced binding activity clearly emerged (Figure S2). Hence, the central lipocalin coding region of the mixed phasmid preparation was subcloned on a vector for the expression of the soluble lipocalin variants in the periplasm of *E. coli*,[27] followed by small scale expression of individual clones. Subsequent ELISA screening of 184 independent clones revealed one lipocalin variant, T4B11, that showed strong binding activity towards muTfR-ED (Figure S2). This Anticalin candidate exhibited 18 amino acid exchanges compared to wtLcn2 (Figure 2A).

After subcloning of the corresponding expression cassette on the plasmid pNGAL118,[24] the protein was produced with a C-terminal His_6-tag in *E. coli* JM83 in 2 L shake flask culture. The soluble monomeric lipocalin variant was purified from the periplasmic cell fraction via IMAC and SEC. As expected, the analytical SEC determined an apparent molecular weight of 22.8 kDa for T4B11, similar to that of the recombinant Lcn2 (23.1 kDa; Figure 2B). To verify the correct protein size and the proper formation of the single structural disulfide bond in the engineered lipocalin, its precise molecular mass was measured by ESI-MS, resulting in a value of 21 453.7 Da, which perfectly matched the calculated mass of 21 454.4 Da for the mature oxidized protein (Figure S4A). To determine the target affinity of the selected Anticalin, SPR real-time analysis was performed with immobilized muTfr-ED on a BIAcore 2000 system, resulting in an equilibrium dissociation constant (K_D) of 13.8 nM (Figure S4B).

Importantly, T4B11 showed a fast dissociation rate constant ($k_{off} = 1.0 \times 10^{-3}\ s^{-1}$) and, consequently, a rather short complex half-life of ~8 min. Thus, its binding activity towards muTfR is highly dynamic and comparable to the natural ligand, muTf (showing here biphasic dissociation kinetics with half-lives of ~1 and ~3 min, respectively). Likewise, the TfR dissociation kinetics of this Anticalin is only moderately slower than the one of the scFv 8D3 ($k_{off} = 7.8 \times 10^{-3}\ s^{-1}$; Figure 1E), a different protein ligand of TfR which was successfully applied for RMT-based drug delivery into mouse brains.[11c,d] Nevertheless, the moderate association rate constant of T4B11, its comparably low expression yield of 0.22 mg/l × OD_{550} and some tendency of aggregate formation prompted further improvement.

Maturation and selection of TfR-specific Anticalins from a random mutagenesis library

To improve the protein yield, stability and target affinity, the selected lipocalin variant T4B11 was subjected to maturation by employing bacterial cell surface display (Figure S3).[28] To this end, random mutagenesis libraries based on T4B11 were generated by error-prone PCR at a low mutation rate and

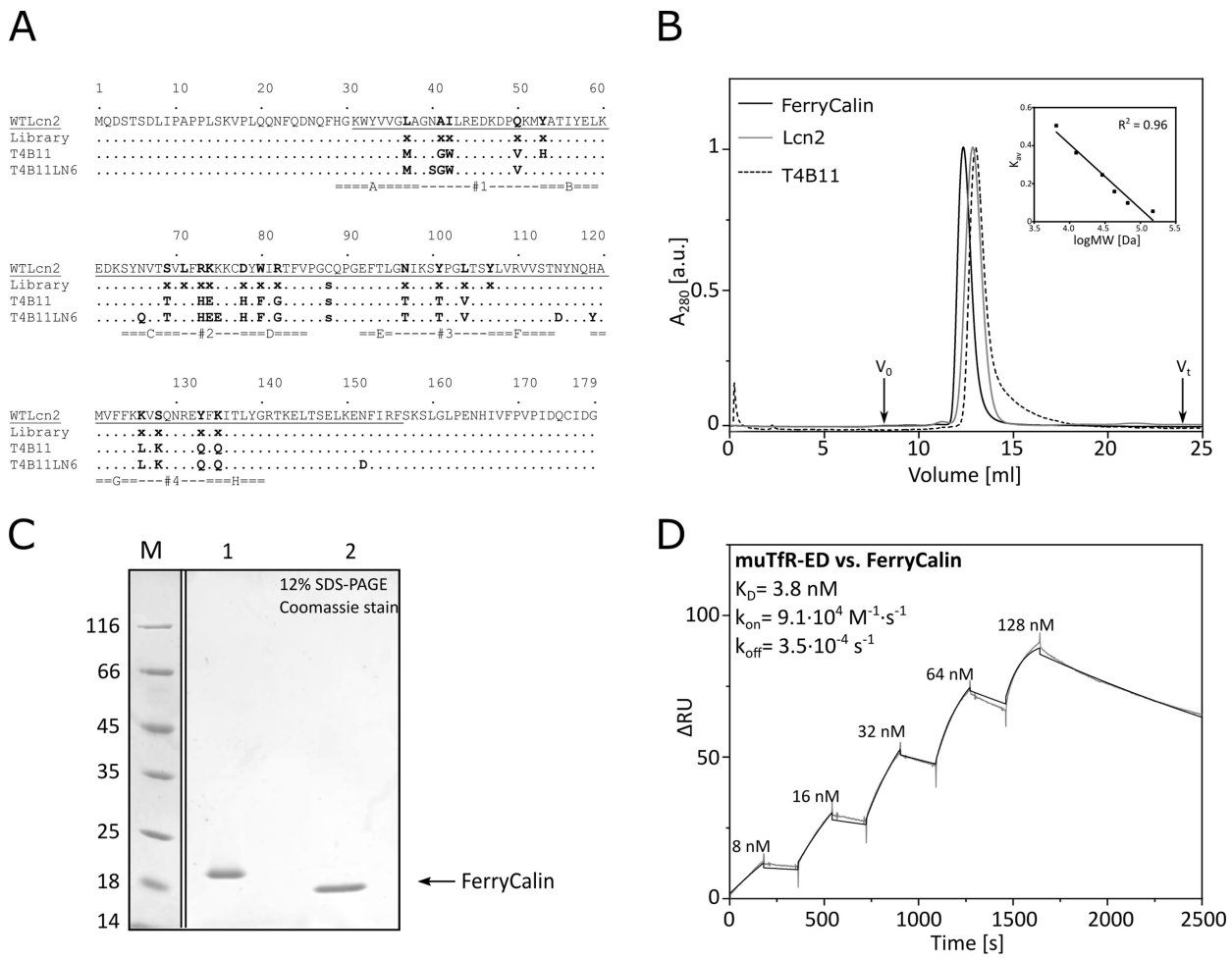

Figure 2. Biochemical and biophysical properties of the muTfR-specific FerryCalin. (A) Amino acid sequence alignment of the selected Anticalins T4B11 and T4B11LN6 (FerryCalin) with the wild-type Lcn2 sequence. Randomized positions in the Lcn2 combinatorial library are indicated by x, identical residues in the variants are represented as dots. The two amino acid substitutions Q28H and C87S served to introduce a second *Bst*XI restriction site and to remove the unpaired exposed Cys side chain from the Lcn2 scaffold, respectively. The central gene cassette flanked by the pair of *Bst*XI sites is underlined. (B) Preparative SEC of the FerryCalin in comparison with T4B11 and wtLcn2, confirming similar apparent molecular masses (~22 kDa) and the absence of oligomers or aggregates. (C) SDS-PAGE analysis of the FerryCalin under reducing (1) and non-reducing (2) conditions. (D) SPR real-time binding analysis of the FerryCalin versus the immobilized muTfR-ED (ΔRU ~800), demonstrating high affinity with relatively fast association and dissociation rates.

subcloned on the vector pNGAL146.[27] Transformation of *E. coli* JK321[29] yielded ~3.5×10^9 independent clones. After the mutagenesis, the recombinant gene expression was induced in the pooled culture at 37 °C – instead of 30 °C[28] – to select on more robust folding stability of encoded protein mutants. The bacterial library displaying the lipocalin variants was then incubated with the biotinylated muTfR-ED/muTf·Fe^{3+} complex and, after that, with a fluorescent streptavidin/phycoerythrin (PE) conjugate, whereby the target concentration was decreased every second cycle in order to raise the stringency of selection (Figure S3C). Finally, FACS was performed for ~6×10^6 cells on a FACSaria instrument, and 2% of those events corresponding to the highest signals in the PE channel were sorted (see Figure S3).

Enrichment of lipocalin variants with binding activity towards muTfR-ED was observed beginning at the second FACS cycle of the first error-prone PCR (not shown). However, the signal was not significantly increased if compared to the original clone T4B11 (under the same conditions) after lowering the receptor concentration from 100 nM to 10 nM and, finally, to 1 nM in the fifth FACS cycle. Hence, a second error-prone mutagenesis and FACS campaign were performed. After completion of selection cycle 5 of this second mutagenesis library the fluorescence signal for the binding of muTfR was still not significantly better if compared to T4B11, and a last round of error-prone mutagenesis and FACS were carried out.

Hence, each mutagenesis PCR had introduced 1–2 additional mutations into the central *Bst*XI-flanked gene cassette of the selected variants, culminating in 4–6 nucleotide exchanges per gene over in total three rounds of error-prone PCR. This time, after the second FACS cycle an enrichment of lipocalin variants with increased binding activity towards muTfR compared to the original T4B11 variant was observed (not shown), and this became even more pronounced with decreasing target concentration in the subsequent cycles (100 nM in cycle 1 and 2, 10 nM in cycle 3 and 4, 1 nM in cycle 5). After cycle 5, the

selected bacteria were plated on agar and 15 colonies were propagated and investigated for muTfR binding activity using single clone FACS analysis.

For all 15 clones significantly higher binding activity towards muTfR-ED with reference to the bacteria expressing T4B11 was evident (Figure S4C). Nine mutants with the best binding activities and highest bacterial surface expression levels were chosen for DNA sequencing, leading to the Anticalin candidates T4B11LN1-9, which differed from T4B11 in 4–6 amino acid positions (Figure S5).

After subcloning of the central lipocalin coding region onto the expression plasmid pNGAL118, the Anticalin candidates were produced in *E. coli* JM83 as soluble proteins with a C-terminal His_6-tag using 2 L shake flask cultures. Purification was achieved from the periplasmic cell fraction via IMAC and SEC. The analytical SEC showed only minor residual aggregates, allowing efficient isolation of the homogenous monomeric protein solutions (Figure 2B). The kinetic properties of the variants were again determined via SPR real-time analysis. Some of the selected candidates showed comparable association and dissociation kinetics to T4B11 (LN3 and LN9) or to the 8D3 scFv (LN6.3) while other variants showed an even higher (LN6) or a lower (LN4) affinity towards muTfR-ED (Table S1). All of the maturated Anticalins exhibited increased bacterial surface display in the FACS analysis and were less prone to aggregation (as indicated by the absence of a peak close to V_0 in the preparative SEC).

Biochemical characterization of FerryCalin

The variant T4B11LN6, which differs from T4B11 by 5 amino acid exchanges (Figure 2A), stood out after these initial expression and binding studies due to its higher target affinity as well as protein stability and was chosen for further analysis, dubbed FerryCalin. As expected, its apparent molecular size of 24.8 kDa (Figure 2B), as determined by analytical SEC, was similar to the ones of the recombinant wtLcn2 (23.1 kDa) and the parental variant T4B11 (22.8 kDa). Its precise molecular mass was verified by ESI-MS, resulting in a value of 21 497.0 Da (compared to a calculated mass of 21 496.4 Da for the oxidized protein). SDS-PAGE confirmed high purity of the protein preparation and proper formation of the intramolecular disulfide bridge, in line with the MS measurement (Figure 2C).

Again, SPR real-time analysis was performed to determine the kinetic and thermodynamic binding constants of this Anticalin, resulting in a K_D value of 3.8 nM. Notably, FerryCalin showed faster association and slightly slower dissociation rate constants ($k_{on} = 9.12 \times 10^4\ M^{-1}\ s^{-1}$; $k_{off} = 3.48 \times 10^{-4}\ s^{-1}$) than T4B11 and, consequently, an increased complex dissociation half-life of ~33 min (Figure 2D). Nevertheless, its binding activity towards muTfR is highly dynamic and the dissociation rate is in an acceptable range for the Anticalin to be further investigated in vitro and in vivo as a potential brain shuttle molecule. Importantly, the expression yield of FerryCalin was drastically increased to 4.15 mg/l×OD_{550}, which is 20-fold higher than for T4B11.

Epitope mapping and competition analysis of FerryCalin with muTf·Fe^{3+} towards TfR binding

To avoid interference with the natural iron transport process and to enable simultaneous binding to TfR by both the Anticalin and the natural ligand muTf·Fe^{3+}, we conducted a series of SPR competition experiments. First, the procedure was verified by control experiments using the 8D3 scFv fragment,[11c] for which binding to TfR at an epitope different from the binding site for Tf is known (Figures S1C, D).[11d,30] To this end, first 1 μM muTf·Fe^{3+} was injected onto the sensorchip with the immobilized muTfR-ED, thus completely saturating the receptor, which was followed by application of a solution containing both 1 μM muTf·Fe^{3+} and 0.128 nM 8D3 scFv. For comparison, 0.128 nM 8D3 scFv was injected separately (Figure S1C). The increase in the response units (ΔRU) for the solution containing both proteins compared to muTf·Fe^{3+} alone matched the ΔRU after injection of the 8D3 scFv, thus indicating simultaneous binding of both proteins.

In an analogous experiment with FerryCalin, non-competitive binding with regard to muTf·Fe^{3+} was observed as well (Figure 3). This was evident from the additive resonance trace when comparing the injected mixture of 0.5 μM FerryCalin and 0.128 μM muTf·Fe^{3+} with either 0.128 μM muTf·Fe^{3+} (Figure 3A) or 0.5 μM FerryCalin alone (Figure 3B). To further verify mutually distinct binding sites of the 8D3 scFv and FerryCalin, we first injected 0.5 μM FerryCalin in order to saturate the immobilized receptor, followed by an injection of a solution containing a mixture of 0.5 μM FerryCalin and 0.128 μM 8D3 scFv (Figure S1D). For comparison, 0.128 μM 8D3 scFv was injected separately. In both experiments, the observed increase in response units for the protein mixture matched the ΔRU value if either muTf·Fe^{3+} or the 8D3 scFv alone was applied. Hence, FerryCalin recognizes an epitope which is neither affected by conformational changes of the receptor upon muTf·Fe^{3+} binding nor it directly competes with the binding of either the natural muTfR ligand or the previously described 8D3 scFv.

In the light of the three N-glycosylation sites on the muTfR-ED (Asn^{253}, Asn^{319} and Asn^{725}; see Figure 4C, highlighted in red), which most likely do not form part of the epitope, as well as the non-interference with the known muTf·Fe^{3+} binding site, the Anticalin probably engages with muTfR at a lateral position of the apical domain or the protease-like domain.[31] To more precisely identify the binding site on muTfR, a peptide epitope mapping was performed with FerryCalin using the SPOT technique.[32] Arrays of consecutive 16mer peptides, each overlapping by 4 amino acids (in total 174), thus covering the entire amino acid sequence of the muTfR-ED, were synthesized on a hydrophilic membrane (Figure 4A). These arrays were probed with the purified Anticalin, whose binding was detected with an antibody-enzyme conjugate. In this assay, specific signals were only observed for a pair of peptides covering positions 285–305 of the mature muTfR sequence. To narrow down the minimal epitope on muTfR, this sequence region was further analyzed by spotting overlapping 12mer peptides (not shown). As result, a single binding site for the FerryCalin on muTfR was

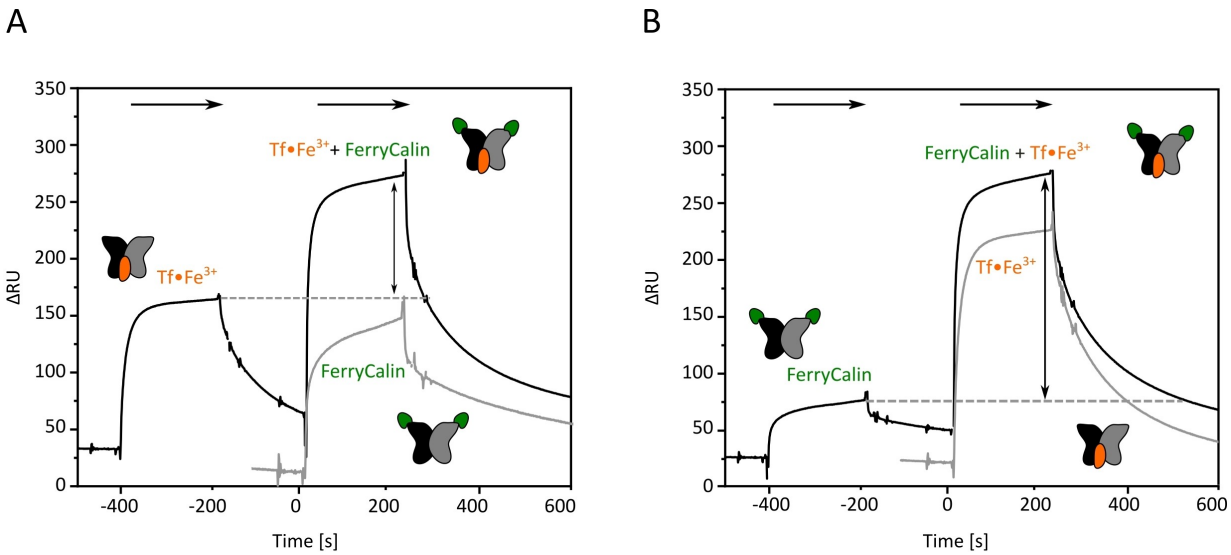

Figure 3. SPR competition analysis between the FerryCalin and muTf·Fe^{3+} for muTfR-ED. (A) muTfr-ED (ΔRU ~800) was immobilized on a sensorchip and its binding sites were first saturated by injection (horizontal arrow) of 0.128 μM muTf·Fe^{3+}, followed by injection of a solution containing both 0.128 μM muTf·Fe^{3+} and 0.5 μM Anticalin T4B11LN6 (FerryCalin); for comparison, 0.5 μM FerryCalin was injected separately (grey) in the absence of muTf·Fe^{3+}. (B) muTfr-ED (ΔRU ~800) was immobilized on a sensorchip and its binding sites were first saturated with 0.5 μM FerryCalin, followed by injection of a solution containing both 0.5 μM FerryCalin and 0.128 μM muTf·Fe^{3+}; for comparison, 0.128 μM muTf·Fe^{3+} was injected separately (grey) in the absence of the Anticalin. Additional increases in ΔRU during the second injection are indicated by vertical arrows for both measurements, thus demonstrating simultaneous binding of both analytes to the muTfr-ED.

identified comprising the 9mer sequence "VVEADLALF" (Figure 4B). Indeed, in the crystal structure of muTfR[33] this linear epitope is exposed on the protein surface of the homodimer and located remote from the recognition site of the endogenous ligand muTf·Fe^{3+} (Figure 4C). Likewise, the epitope does not coincide with the binding site for heavy-chain ferritin as described for the homologous human TfR (residues 195–215 and 343–348).[12]

Conclusions

Taken together, the Anticalin T4B11 and its more stable variants, including FerryCalin (T4B11LN6), constitute novel protein reagents that specifically recognize muTfR and show favorable binding characteristics in terms of varying affinity (K_D values in the range of 3.8 to 51.3 nM; cf. Table S1) and highly dynamic association/dissociation kinetics. Hence, these Anticalins offer promising properties to exploit the endogenous RMT activity of the muTfR at the BBB without affecting its interaction with the plasma iron transport protein muTf. Due to their small and robust single-domain architecture, the monovalent binding mode, absence of Fc-mediated effector functions and generally flexible molecular formatting options (with freely accessible N- and C-termini for fusion or conjugation with pharmacologically active compounds), Anticalins provide important benefits over conventional antibodies for brain drug delivery. Furthermore, the pharmacokinetics of these fusion proteins can be easily adjusted by combination with so-called PAS tags[34] of variable lengths to increase the plasma half-life. Thus, the most promising Anticalin candidates, especially FerryCalin, expand the tool set to enhance brain delivery of conjugated therapeutic or diagnostic agents, which will be further investigated in future in vitro and in vivo studies.

Experimental Section

Soluble production and purification of the biotinylated murine TfR extracellular domain: The coding sequence for the extracellular domain of the murine transferrin receptor 1 (muTfR-ED; UniProt ID: Q62351, residues Cys^{89}–Phe^{763}) was amplified from the plasmid pcDNA5-muTfR-FRT-TO (Thermo Fisher Scientific, St. Leon-Rot, Germany) using the primers 5′-GCA TGA AGC GCT TCT AAG CGT GTA GAA CAA AAA GAG GAG-3′ and 5′-GCA TTA GCG GCC GCA AGC TTA AAA CTC ATT GTC AAT ATT CCA AAT GTC AC-3′. The first primer was designed to introduce a 5′ *Afe*I restriction site as well as to replace the codon for Cys^{89} (TGT) by a codon for Ser (TCT) in order to obtain a well-defined homodimeric protein preparation with only one disulfide bond within the muTfR-ED stalk region, whereas the second primer introduced a 3′ *Hin*dIII restriction site downstream of the stop codon to allow subcloning on the plasmid pDSG102 (IBA Lifesciences, Göttingen, Germany), thus yielding the expression plasmid pDSG-BM40-His_6-BAP-muTfR-ED-Igk-BirA-*Strep*DEL[35] (Figure 1).

Production of the biotinylated muTfR-ED, as a disulfide-crosslinked homodimer, in human embryonic kidney (HEK) 293E cells (MEXi expression system; IBA Lifesciences) was essentially performed as recommended by the supplier. Briefly, cells were cultivated in MEXi cultivation medium supplemented with 50 mg/l G-418 and 8 mM L-alanyl-L-glutamine at 37 °C under humidified 5% CO_2 atmosphere. 5×10^6 cells/ml dispersed in 250 mL MEXi transfection medium were transfected with 5 μg plasmid DNA per 1×10^6 cells, which was previously mixed at a 1:3 mass ratio with 25 kDa linear polyethylenimine (PEI; Polysciences Europe, Eppelheim, Germany) in MEXi transfection medium. After 4 h incubation at 37 °C, 500 mL

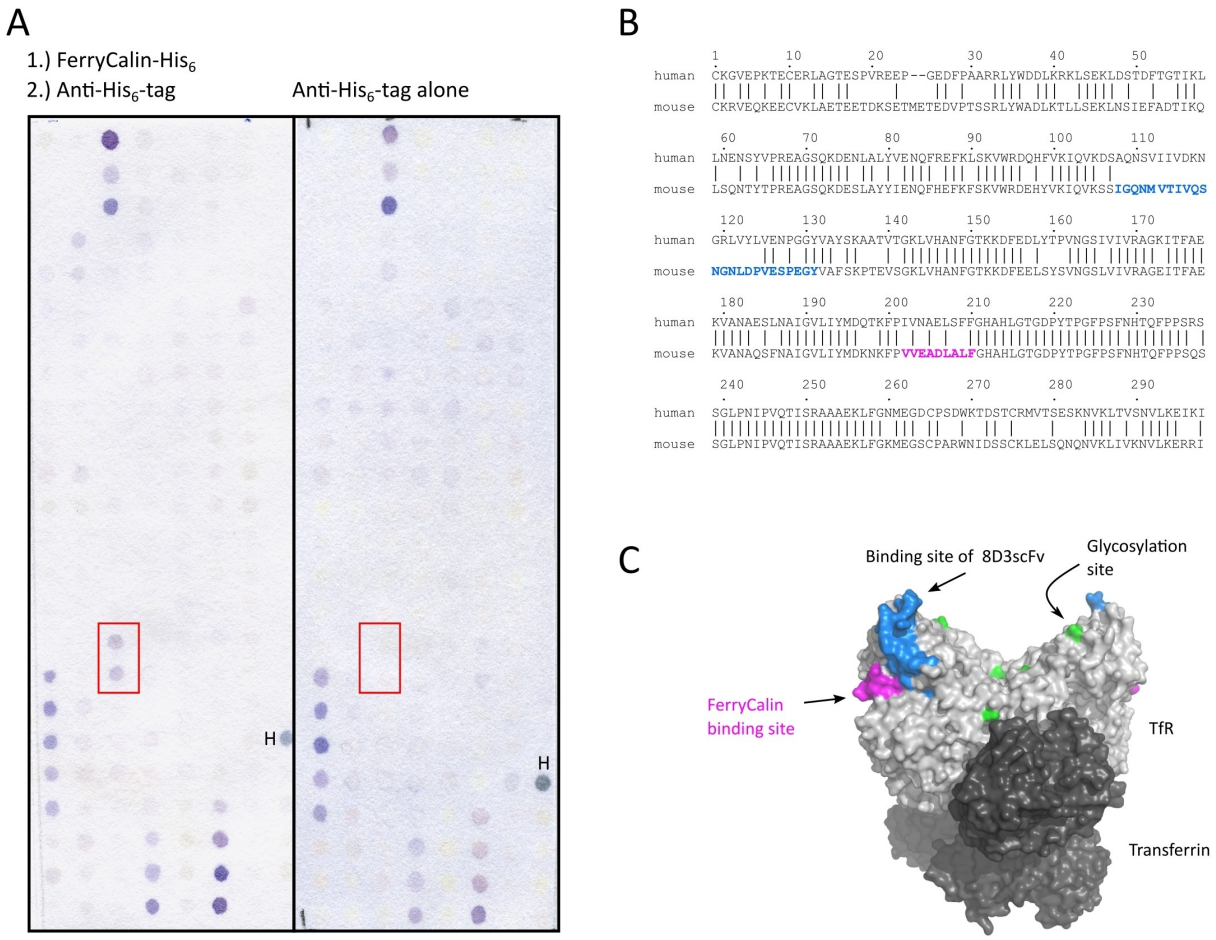

Figure 4. Epitope mapping of the FerryCalin on the ectodomain of muTfR. (A) A SPOT membrane carrying an array of 16mer peptides, each overlapping by 4 amino acids, thus covering the entire amino acid sequence of the murine TfR ectodomain, was incubated with either 2 μM FerryCalin-His_6 and an anti-6×His-tag/AP conjugate (1:20,000) or, as a negative control, with the secondary reagent alone. Specific signals for two spots that only emerged on the first membrane represent the linear epitope sequence that is recognized by the Anticalin: DKNK**FPVVEADLALFG**HAHL (residues in common to both spots are printed bold). To confirm the specificity of the secondary reagent, a His_6 peptide was also included in the array (labeled H, shifted by one position in the negative control). (B) Sequence alignment of the human and murine TfRs with the epitopes of the FerryCalin (magenta, residues 202–210 of the muTfR ectodomain, corresponding to 292–300 in the full length sequence) and of the 8D3 scFv (blue, residues 108–131)[11d] highlighted. (C) Surface location of the binding sites of the FerryCalin (magenta) and of the 8D3 scFv (blue) on the TfR (light grey) in relation to the one for its natural ligand muTf·Fe^{3+} (displayed dark grey) based on the crystal structure (PDB ID: 1SUV). The experimentally validated N-glycosylation sites in the muTfR-ED (Asn253, Asn319 and Asn725) are highlighted green.[20]

of fresh MEXi cultivation medium was added and transient secretory protein expression was continued for 4 days.

After sedimentation of the cells by centrifugation, the supernatant was dialyzed against immobilized metal ion affinity chromatography (IMAC) buffer (20 mM Tris/HCl pH 8.0, 500 mM NaCl), and IMAC was performed on a Ni(II)-charged HisTrap HP column (GE Healthcare, Munich, Germany). After applying a linear concentration gradient of 0–300 mM imidazole/HCl in IMAC buffer the elution fractions were pooled and subsequently applied to a 5 mL affinity column containing the streptavidin mutant 1.6 (streptavidin mutant 1[18] with the additional mutations N23A and S27A) which allows reversible binding of biotinylated proteins. After competitive elution by applying 5 mM D-biotin in the same buffer, preparative size-exclusion chromatography (SEC) was performed on a 24 mL Superdex 200 10/300 GL column (GE Healthcare) using PBS (4 mM KH_2PO_4, 16 mM Na_2HPO_4, 115 mM NaCl, pH 7.4) as running buffer.

SDS-PAGE was performed using a high molarity Tris buffer system,[36] followed by staining with Coomassie brilliant blue, using an SDS sample buffer with or without 2-mercaptoethanol. Western blotting onto a polyvinylidene difluoride (PVDF) membrane was carried out as previously described.[37] For detection of the biotinylated muTfR-ED, an ExtrAvidin/alkaline phosphatase (AP) conjugate (Sigma–Aldrich, Munich, Germany) was applied at a dilution of 1:5000, followed by chromogenic reaction.

Production and purification of the 8D3 single chain variable fragment (scFv): The coding region for the scFv fragment derived from the monoclonal antibody 8D3[11a,21] was obtained by gene synthesis (GeneArt/Thermo Fisher Scientific, St. Leon-Rot, Germany) with a nucleotide sequence optimized for expression in *E. coli*. To facilitate the preparation of the 8D3 antibody fragment in different formats, we introduced unique restriction sites for *Pst*I and *Bst*EII as well as *Sac*I and *Xho*I at the beginning and the end of the V_H and V_L regions, respectively.[38] The coding region for the 8D3 scFv was subcloned on a derivative of pASK75 which provides an N-terminal OmpA signal peptide for periplasmic secretion as well as the *Strep*-tag II at the C-terminus for affinity purification.[39] The resulting plasmid, pASK98-8D3scFv-strep, was used to transform *E. coli*

JM83,[40] followed by recombinant gene expression in 2 L shake flask cultures and purification via Strep-Tactin affinity chromatography according to published procedures.[39] Finally, the homogenous monomeric protein was isolated by SEC on a 24 mL Superdex 75 10/300 GL column in PBS and its purity was confirmed by SDS-PAGE as above.

Analytical size exclusion chromatography: Analytical SEC was performed on a 24 mL Superdex 200 or 75 10/300 GL column using PBS as running buffer at a flow rate of 0.5 mL/min. The Superdex 200 column was calibrated with the following standard proteins (Sigma–Aldrich): thyroglobulin (TG, 669 kDa), apoferritin (Af, 443 kDa), alcohol dehydrogenase (ADH, 150 kDa), bovine serum albumin (BSA, 66 kDa), carbonic anhydrase (CA, 29 kDa), cytochrome *c* (Cy, 12.4 kDa) and aprotinin (Ap, 6.5 kDa) whereas for the Superdex 75 column BSA, ovalbumin (Oa, 43 kDa), ribonuclease A (RA, 13.7 kDa), Cy and Ap were used. Blue dextran was applied to determine the void volume of each column. Based on the elution volumes, the partition coefficients K_{av} were calculated and used to interpolate the apparent molecular masses of the analyte proteins via linear regression on a semilogarithmic scale.

ESI mass spectrometry: Mass spectra of purified proteins were measured on a maXis time-of-flight mass spectrometer with an electrospray ionization (ESI) source (Bruker Daltonics, Bremen, Germany) in the positive ion mode as previously described.[41] To this end, the purified protein was dialyzed against 10 mM ammonium acetate pH 6.6, followed by the addition of 50% (v/v) methanol and 1% (v/v) formic acid, and directly applied via a syringe pump at 180 μL/h. The following conditions for the ion transfer were used: 3400 V capillary voltage, 500 V endplate offset, 4 L/min dry gas at 200 °C, 0.3 bar nebulizer pressure and 3 eV collision energy. Raw spectra were deconvoluted with the Bruker Compass Data Analysis Software using the MaxEnt algorithm.[42]

Phage display selection and bacterial production of muTfR-specific lipocalin variants: The purified muTfR-ED (2.6 μM in PBS) was mixed at a 2-fold molar concentration with iron-charged muTf (muTf·Fe^{3+}; Rockland, Limerick, PA) and incubated for 1 h at 20 °C. Phage display selection was performed using an Lcn2-based random library as previously described.[24,27] To this end, the biotinylated recombinant muTfR-ED (300 nM for all cycles) in complex with muTf·Fe^{3+} was captured, in an alternating manner, on paramagnetic beads coated with NeutrAvidin (Sigma–Aldrich), for cycles 1, 3 and 5, or with streptavidin (Thermo Fisher Scientific), for cycles 2, 4 and 6, and then incubated for 60 min with the phagemid library (starting titer 1×10^{12}). After extensive washing, bound phagemids were eluted under denaturing conditions by applying 4 M urea in PBS.

Following infection of XL1-blue cells,[43] the pooled phasmid DNA was prepared and, after six cycles, subcloned on the expression plasmid pNGAL98 for subsequent high-throughput ELISA screening from *E. coli* microcultures secreting the soluble lipocalin variants carrying the C-terminal *Strep*-tag II.[24] To this end, the periplasmic extract was each prepared from a 2 mL culture in a deep-well microtiter plate as previously described[24] and transferred to a 96-well MaxiSorp plate (Thermo Fisher Scientific) which had been coated with 10 μg/ml *Strep*MAB-Immo (IBA Lifesciences) and blocked. After 1 h incubation and subsequent washing steps, the bound lipocalin variants were incubated with 300 nM of either biotinylated muTfR-ED, chemically biotinylated ovalbumin (Sigma–Aldrich) or with PBS, followed by detection of the bound target protein using ExtrAvidin/AP conjugate (Sigma–Aldrich). Signals were developed with 0.5 mg/ml p-nitrophenyl phosphate in AP buffer (0.1 M NaCl, 5 mM $MgCl_2$, 0.1 M Tris/HCl, pH 8.8) and the absorbance was measured at 405 nm using a Synergy 2 photometer (BioTek Instruments, Winooski, VT).

For the preparative production of the soluble lipocalin variants – then equipped with a His_6-tag – in *E. coli* JM83, the coding region was subcloned on the plasmid pNGAL118[24] and cultivated at the 2 l culture scale. After periplasmic protein extraction according to published procedures[24] the recombinant protein was isolated by IMAC using a 5 mL Ni(II)-charged HisTrap HP column and further purified by SEC in PBS on a 24 mL Superdex 75 10/300 GL column, followed by analysis via SDS-PAGE.

Affinity maturation via bacterial surface display: A second generation Anticalin library was generated by error-prone PCR based on the Anticalin T4B11 that was obtained from the first anti-TfR phage display selection campaign described above using the GeneMorph II random mutagenesis kit (Agilent Technologies, Mannheim, Germany). Initially, the mutation N65Q was inserted into the coding region of T4B11 to avoid unwanted glycosylation at the corresponding sequon during later expression in mammalian cells. The resulting plasmid, pNGAL118-T4B11(N65Q)-His_6, was then used as template for the error-prone PCR according to the manufacturer's protocol. Shortly, 500 ng of the plasmid DNA was used as template together with the primers 5′-CAG GAC AAC CAA TTC CAT GGG-3′ and 5′-GGA GGC CCA GAG ATT TGG-3′, which flank the central coding region of the mutated lipocalin, in order to introduce 1–2 nucleotide exchanges per gene in the course of 20 reaction cycles. The PCR product was digested with *Bst*XI, isolated and inserted into the plasmid pNGAL146,[27] which encodes a fusion protein between Lcn2 and the β-domain of the bacterial autotransporter EspP. The resulting Anticalin library was used for transformation of electro-competent *E. coli* JK321 cells,[29] followed by plating on LB/amp agar plates.

Bacterial cultivation, incubation with the target protein, staining and fluorescence-activated cell sorting (FACS) were carried out as previously described.[28] In brief, colonies were scraped from the agar plate, suspended in 50 mL LB/amp medium and shaken for 1 h at 37 °C. 1 mL of this culture was used to inoculate a 50 mL LB/amp overnight culture at 30 °C, which in turn was used the next day to inoculate 50 mL LB/amp at 37 °C with a starting $OD_{550}=0.15$. Gene expression was induced at $OD_{550}=0.5$ by addition of 10 ng/ml anhydrotetracycline (aTc) for 2.5 h. Cells from 200 μL of this culture were spun down in an Eppendorf tube for 3 min at 4 °C, washed once in PBS and resuspended in 100 μL 100 nM biotinylated muTfR-ED in PBS supplemented with 200 nM muTf·Fe^{3+}. After 1 h incubation on ice, the bacteria were incubated with 50 μL PBS containing 25 μg/ml streptavidin/phycoerythrin conjugate (SA/PE; BD Biosciences, Heidelberg, Germany) and with 3 μM DY634-labelled A3C5 Fab fragment directed against a peptide tag serving as linker in the lipocalin-autotransporter fusion protein.[28] Following 10 min incubation on ice, the bacteria were finally centrifuged, washed once with 0.5 mL PBS and then applied to a FACSAria cell-sorting system (BD Biosciences).

For fluorescence detection of phycoerythrin (PE), a 488 nm laser diode and a 530/30 band pass filter were used, while DY634 was detected using a 633 nm HeNe laser and a 660/20 band pass filter. In each of the five selection rounds the fraction comprising 0.1–1% of cells showing the highest fluorescence in the PE channel were sorted and propagated for the next cycle. The stringency of selection was gradually increased by lowering the concentration of the muTfR-ED target (100 nM in cycles 1 and 2; 10 nM in cycles 3 and 4; 1 nM in cycle 5), which was always preincubated with a 2-fold molar amount of muTf·Fe^{3+}. To obtain further improved Anticalin variants, we used the selected population from cycle 5 for another round of error-prone mutagenesis in order to introduce additional 1–2 nucleotide mutations into the *Bst*XI-flanked gene cassettes of the mutants, followed by FACS with increasing stringency by lowering the concentration of the muTfR-ED target after every second cycle, as mentioned above. This was repeated a

third time, so in total approx. 4–6 nucleotide exchanges were introduced into the lipocalin variants on average. Finally, single selected bacterial clones were analyzed by DNA sequencing of the central coding region (flanked by the *Bst*XI restriction sites) as well as by individual cultivation and FACS analysis. For preparative production and functional characterization of promising Anticalin candidates, the *Bst*XI gene cassette was subcloned on pNGAL118 and further processed as described above.

Biomolecular interaction analysis: Real-time surface plasmon resonance (SPR) analyses were performed on a BIAcore 2000 system (BIAcore, Uppsala, Sweden) using HBS/T (20 mM Hepes/NaOH pH 7.5, 150 mM NaCl, 0.005% v/v Tween-20) as running buffer at 25 °C. NeutrAvidin (Sigma-Aldrich) was immobilized onto a carboxymethyl dextran-coated CM5 sensor chip (GE Healthcare) via amine coupling chemistry as previously described,[24] and the biotinylated muTfR-ED was captured on the functionalized surface to achieve a resonance response of $\Delta RU \approx 250$. A 1:2 dilution series of the respective ligand or binding protein (Anticalin or scFv) was injected using multiple cycle kinetics. The raw data were corrected by subtraction of (i) the corresponding signals measured for the control channel and (ii) an averaged baseline determined from three buffer blank injections.[44] To determine the rate constants of association and dissociation, k_{on} and k_{off}, the resulting sensorgrams were analyzed by global fitting with BIAevaluation software (ver. 4.1, BIAcore) using a 1:1 Langmuir binding model, also correcting for a baseline drift (in case of the lipocalin variant T4B11LN6 and of the scFv 8D3) or accounting for a heterogeneous ligand (in case of muTf·Fe^{3+}). The equilibrium dissociation constant was calculated as $K_D = k_{off}/k_{on}$.

SPOT synthesis of immobilized peptide arrays and identification of the peptide epitope: Arrays of 16mer peptides overlapping by 4 amino acids, in total 174, thus covering the entire amino acid sequence of the murine TfR ectodomain, as well as overlapping 12mer peptides covering the narrower epitope region, were prepared according to the SPOT technique[32] using an automated MultiPep RS peptide synthesizer (Intavis, Cologne, Germany). Briefly, the peptides were synthesized on an amino-PEG500-derivatized cellulose membrane (Intavis) as distinct spots. A β-alanine dipeptide was used as spacer between the C-terminus of each peptide and the membrane support. The peptides were extended stepwise via standard fluorenyl methoxycarbonyl solid-phase peptide synthesis, followed by final cleavage of the side chain protecting groups using trifluoroacetic acid. All peptides were N-terminally acetylated. Sequence files were generated with the software DIGEN (Jerini, Berlin, Germany).

To detect binding activity of the Anticalin on the SPOT membrane,[45] the membrane was initially blocked in Membrane Blocking Solution (MBS: 50 mM Tris/HCl pH 8.0, 137 mM NaCl, 2.7 mM KCl, 0.05% v/v Tween-20, 1% w/v sucrose) for 10 min. Then, the membrane was incubated for 1 h with 2 μM protein solution in MBS, followed by incubation for 1 h with an anti-6×His-tag antibody AP conjugate (arigo biolaboratories, Hamburg, Germany) in MBS at a dilution of 1:20,000. After two washing steps with TBS/T (50 mM Tris/HCl pH 8.0, 137 mM NaCl, 2.7 mM KCl, 0.05% v/v Tween-20) the signals were developed in 20 mL AP buffer with the addition of 60 μL BCIP (50 mg/ml 5 bromo-4-chloro-3-indolylphosphate p-toluidine salt in DMF) and 10 μL NBT (75 mg/ml 2,2′-bis(4-nitrophenyl)-5,5′-diphenyl-3,3′-(3,3′-dimethoxy-4,4′-diphenylene)ditetrazolium chloride in 70% v/v DMF) for approximately 8 min. For repeated use, the membrane was regenerated with 2-mercaptoethanol/SDS reagent according to a published protocol[37] and the quantitative removal of bound protein was confirmed by detection with the anti-6×His-tag antibody AP conjugate.

Supporting Information

Additional references cited within the Supporting Information.[27–28,46–47]

Acknowledgements

This work was supported by the German Research Foundation (DFG) in frame of the Collaborative Research Centre 824 (project A08). The authors wish to thank Prof. Martin Klingenspor (TU Munich) for providing the pcDNA5-muTfR-FRT-TO plasmid and Stefan Achatz and Corinna Brandt for performing MS analyses and experimental support. Anticalin® is a registered trademark of Pieris Pharmaceuticals GmbH. Open Access funding enabled and organized by Projekt DEAL.

Conflict of Interest

A. Sk. is co-founder and shareholder of Pieris Pharmaceuticals, Inc.

Data Availability Statement

The data that support the findings of this study are available in the Supporting Information of this article.

Keywords: blood brain barrier · drug delivery · lipocalin · protein engineering · TfR

[1] a) W. M. Pardridge, *Brain Drug Targeting: The Future of Brain Drug Development*, Cambridge University Press, Cambridge, **2001**; b) Y. Serlin, I. Shelef, B. Knyazer, A. Friedman, *Semin. Cell Dev. Biol.* **2015**, *38*, 2–6.
[2] I. St-Amour, I. Pare, W. Alata, K. Coulombe, C. Ringuette-Goulet, J. Drouin-Ouellet, M. Vandal, D. Soulet, R. Bazin, F. Calon, *J. Cereb. Blood Flow Metab.* **2013**, *33*, 1983–1992.
[3] W. M. Pardridge, *Nat. Rev. Drug Discovery* **2002**, *1*, 131–139.
[4] J. Paterson, C. I. Webster, *Drug Discovery Today Technol.* **2016**, *20*, 49–52.
[5] M. J. Coloma, H. J. Lee, A. Kurihara, E. M. Landaw, R. J. Boado, S. L. Morrison, W. M. Pardridge, *Pharm. Res.* **2000**, *17*, 266–274.
[6] Y. J. Zuchero, X. Chen, N. Bien-Ly, D. Bumbaca, R. K. Tong, X. Gao, S. Zhang, K. Hoyte, W. Luk, M. A. Huntley, L. Phu, C. Tan, D. Kallop, R. M. Weimer, Y. Lu, D. S. Kirkpatrick, J. A. Ernst, B. Chih, M. S. Dennis, R. J. Watts, *Neuron* **2016**, *89*, 70–82.
[7] a) E. Gammella, P. Buratti, G. Cairo, S. Recalcati, *Metallomics* **2017**, *9*, 1367–1375; b) W. A. Jefferies, M. R. Brandon, S. V. Hunt, A. F. Williams, K. C. Gatter, D. Y. Mason, *Nature* **1984**, *312*, 162–163.
[8] a) D. Sehlin, S. Syvanen, *Eur. J. Nucl. Med. Mol. Imaging* **2019**, *46*, 2848–2858; b) H. Sonoda, H. Morimoto, E. Yoden, Y. Koshimura, M. Kinoshita, G. Golovina, H. Takagi, R. Yamamoto, K. Minami, A. Mizoguchi, K. Tachibana, T. Hirato, K. Takahashi, *Mol. Ther.* **2018**, *26*, 1366–1374; c) J. C. Ullman, A. Arguello, J. A. Getz, A. Bhalla, C. S. Mahon, J. Wang, T. Giese, C. Bedard, D. J. Kim, J. R. Blumenfeld, N. Liang, R. Ravi, A. A. Nugent, S. S. Davis, C. Ha, J. Duque, H. L. Tran, R. C. Wells, S. Lianoglou, V. M. Daryani, W. Kwan, H. Solanoy, H. Nguyen, T. Earr, J. C. Dugas, M. D. Tuck, J. L. Harvey, M. L. Reyzer, R. M. Caprioli, S. Hall, S. Poda, P. E. Sanchez, M. S. Dennis, K. Gunasekaran, A. Srivastava, T. Sandmann, K. R. Henne, R. G. Thorne, G. Di Paolo, G. Astarita, D. Diaz, A. P. Silverman, R. J. Watts, Z. K. Sweeney, M. S. Kariolis, A. G. Henry, *Sci. Transl. Med.* **2020**, *12*, eaay1163.

[9] a) Z. Liu, X. Gao, T. Kang, M. Jiang, D. Miao, G. Gu, Q. Hu, Q. Song, L. Yao, Y. Tu, H. Chen, X. Jiang, J. Chen, *Bioconjugate Chem.* **2013**, *24*, 997–1007; b) F. I. Staquicini, M. G. Ozawa, C. A. Moya, W. H. P. Driessen, E. M. Barbu, H. Nishimori, S. Soghomonyan, L. G. Flores, 2nd, X. Liang, V. Paolillo, M. M. Alauddin, J. P. Basilion, F. B. Furnari, O. Bogler, F. F. Lang, K. D. Aldape, G. N. Fuller, M. Höök, J. G. Gelovani, R. L. Sidman, W. K. Cavenee, R. Pasqualini, W. Arap, *J. Clin. Invest.* **2011**, *121*, 161–173.
[10] P. M. Friden, L. R. Walus, G. F. Musso, M. A. Taylor, B. Malfroy, R. M. Starzyk, *Proc. Natl. Acad. Sci. USA* **1991**, *88*, 4771–4775.
[11] a) K. Kissel, S. Hamm, M. Schulz, A. Vecchi, C. Garlanda, B. Engelhardt, *Histochem. Cell Biol.* **1998**, *110*, 63–72; b) H. J. Lee, B. Engelhardt, J. Lesley, U. Bickel, W. M. Pardridge, *J. Pharmacol. Exp. Ther.* **2000**, *292*, 1048–1052; c) G. Hultqvist, S. Syvanen, X. T. Fang, L. Lannfelt, D. Sehlin, *Theranostics* **2017**, *7*, 308–318; d) J. Niewoehner, B. Bohrmann, L. Collin, E. Urich, H. Sade, P. Maier, P. Rueger, J. O. Stracke, W. Lau, A. C. Tissot, H. Loetscher, A. Ghosh, P. O. Freskgard, *Neuron* **2014**, *81*, 49–60.
[12] L. C. Montemiglio, C. Testi, P. Ceci, E. Falvo, M. Pitea, C. Savino, A. Arcovito, G. Peruzzi, P. Baiocco, F. Mancia, A. Boffi, A. des Georges, B. Vallone, *Nat. Commun.* **2019**, *10*, 1121.
[13] D. Stanimirovic, K. Kemmerich, A. S. Haqqani, G. K. Farrington, *Adv. Pharmacol.* **2014**, *71*, 301–335.
[14] a) J. A. Couch, Y. J. Yu, Y. Zhang, J. M. Tarrant, R. N. Fuji, W. J. Meilandt, H. Solanoy, R. K. Tong, K. Hoyte, W. Luk, Y. Lu, K. Gadkar, S. Prabhu, B. A. Ordonia, Q. Nguyen, Y. Lin, Z. Lin, M. Balazs, K. Scearce-Levie, J. A. Ernst, M. S. Dennis, R. J. Watts, *Sci. Transl. Med.* **2013**, *5*, 183ra157; b) Y. J. Yu, J. K. Atwal, Y. Zhang, R. K. Tong, K. R. Wildsmith, C. Tan, N. Bien-Ly, M. Hersom, J. A. Maloney, W. J. Meilandt, D. Bumbaca, K. Gadkar, K. Hoyte, W. Luk, Y. Lu, J. A. Ernst, K. Scearce-Levie, J. A. Couch, M. S. Dennis, R. J. Watts, *Sci. Transl. Med.* **2014**, *6*, 261ra154.
[15] a) A. Richter, E. Eggenstein, A. Skerra, *FEBS Lett.* **2014**, *588*, 213–218; b) C. Rothe, A. Skerra, *BioDrugs* **2018**, *32*, 233–243; c) F. C. Deuschle, E. Ilyukhina, A. Skerra, *Expert Opin. Biol. Ther.* **2021**, *21*, 509–518.
[16] a) B. Barat, A. M. Wu, *Biomol. Eng.* **2007**, *24*, 283–291; b) M. G. Cull, P. J. Schatz, *Methods Enzymol.* **2000**, *326*, 430–440.
[17] W. Gan, M. LaCelle, R. E. Rhoads, *J. Biol. Chem.* **1998**, *273*, 5006–5012.
[18] S. Voss, A. Skerra, *Protein Eng.* **1997**, *10*, 975–982.
[19] J. Denecke, R. De Rycke, J. Botterman, *EMBO J.* **1992**, *11*, 2345–2355.
[20] B. Wollscheid, D. Bausch-Fluck, C. Henderson, R. O'Brien, M. Bibel, R. Schiess, R. Aebersold, J. D. Watts, *Nat. Biotechnol.* **2009**, *27*, 378–386.
[21] R. J. Boado, Y. Zhang, Y. Wang, W. M. Pardridge, *Biotechnol. Bioeng.* **2009**, *102*, 1251–1258.
[22] A. P. West, Jr., M. J. Bennett, V. M. Sellers, N. C. Andrews, C. A. Enns, P. J. Bjorkman, *J. Biol. Chem.* **2000**, *275*, 38135–38138.
[23] B. E. Eckenroth, A. N. Steere, N. D. Chasteen, S. J. Everse, A. B. Mason, *Proc. Natl. Acad. Sci. USA* **2011**, *108*, 13089–13094.
[24] M. Gebauer, A. Schiefner, G. Matschiner, A. Skerra, *J. Mol. Biol.* **2013**, *425*, 780–802.
[25] M. Gebauer, A. Skerra, *Curr. Opin. Biotechnol.* **2019**, *60*, 230–241.
[26] a) N. L. Anderson, N. G. Anderson, *Mol. Cell. Proteomics* **2002**, *1*, 845–867; b) Q. Q. Si, Y. S. Yuan, Y. Zhi, Q. Tong, L. Zhang, K. Zhang, *Neurosci. Lett.* **2018**, *684*, 42–46.
[27] M. Gebauer, A. Skerra, *Methods Enzymol.* **2012**, *503*, 157–188.
[28] U. Binder, G. Matschiner, I. Theobald, A. Skerra, *J. Mol. Biol.* **2010**, *400*, 783–802.
[29] J. Jose, J. Krämer, T. Klauser, J. Pohlner, T. F. Meyer, *Gene* **1996**, *178*, 107–110.
[30] G. Helguera, S. Jemielity, J. Abraham, S. M. Cordo, M. G. Martinez, J. A. Rodríguez, C. Bregni, J. J. Wang, M. Farzan, M. L. Penichet, N. A. Candurra, H. Choe, *J. Virol.* **2012**, *86*, 4024–4028.
[31] C. M. Lawrence, S. Ray, M. Babyonyshev, R. Galluser, D. W. Borhani, S. C. Harrison, *Science* **1999**, *286*, 779–782.
[32] R. Frank, *J. Immunol. Methods* **2002**, *267*, 13–26.
[33] Y. Cheng, O. Zak, P. Aisen, S. C. Harrison, T. Walz, *Cell* **2004**, *116*, 565–576.
[34] M. Schlapschy, U. Binder, C. Börger, I. Theobald, K. Wachinger, S. Kisling, D. Haller, A. Skerra, *Protein Eng. Des. Sel.* **2013**, *26*, 489–501.
[35] F. C. Deuschle, V. Morath, A. Schiefner, C. Brandt, S. Ballke, S. Reder, K. Steiger, M. Schwaiger, W. Weber, A. Skerra, *Theranostics* **2020**, *10*, 2172–2187.
[36] S. P. Fling, D. S. Gregerson, *Anal. Biochem.* **1986**, *155*, 83–88.
[37] H. Zander, U. Reineke, J. Schneider-Mergener, A. Skerra, *J. Mol. Recognit.* **2007**, *20*, 185–196.
[38] A. Skerra, *Gene* **1994**, *141*, 79–84.
[39] T. G. Schmidt, A. Skerra, *Nat. Protoc.* **2007**, *2*, 1528–1535.
[40] C. Yanisch-Perron, J. Vieira, J. Messing, *Gene* **1985**, *33*, 103–119.
[41] F. C. Deuschle, A. Schiefner, A. Skerra, *Proteins* **2019**, *87*, 693–698..
[42] A. G. Ferrige, M. J. Seddon, S. Jarvis, J. Skilling, R. Aplin, *Rapid Commun. Mass Sp.* **1991**, *5*, 374–377.
[43] W. O. Bullock, J. M. Fernandez, J. M. Short, *BioTechniques* **1987**, *5*, 376–379.
[44] D. G. Myszka, *J. Mol. Recognit.* **1999**, *12*, 279–284.
[45] R. Frank, H. Overwin, in *Epitope Mapping Protocols* (Ed.: G. E. Morris), Humana Press, Totowa, NJ, **1996**, pp. 149–169.
[46] A. Eichinger, S. Rauth, D. Hinz, A. Feuerbach, A. Skerra, *Biol. Chem.* **2022**, *403*, 557–571.
[47] W. Brunder, H. Schmidt, H. Karch, *Mol. Microbiol.* **1997**, *24*, 767–778.

Manuscript received: December 29, 2022
Revised manuscript received: March 29, 2023
Accepted manuscript online: April 2, 2023
Version of record online: April 19, 2023